1-16-2020

Seasonal Variability of the CO2 System in a Large Coastal Plain Estuary

Jaclyn R. Friedman
Virginia Institute of Marine Science

Elizabeth H. Shadwick
Virginia Institute of Marine Science

Marjorie A.M. Friedrichs
Virginia Institute of Marine Science

Raymond G. Najjar

Olivia A. De Meo
Virginia Institute of Marine Science

See next page for additional authors

Recommended Citation

Friedman, Jaclyn R.; Shadwick, Elizabeth H.; Friedrichs, Marjorie A.M.; Najjar, Raymond G.; De Meo, Olivia A.; Da, Fei; and Smith, Juliette L., Seasonal Variability of the CO2 System in a Large Coastal Plain Estuary (2020). *JGR Oceans*, 125(1), e2019JC015609.
10.1029/2019JC015609

JGR Oceans

RESEARCH ARTICLE
10.1029/2019JC015609

Special Section:
Carbon cycling in tidal wetlands and estuaries of the contiguous United States

Seasonal Variability of the CO_2 System in a Large Coastal Plain Estuary

Jaclyn R. Friedman[1], Elizabeth H. Shadwick[1,2], Marjorie A.M. Friedrichs[1], Raymond G. Najjar[3], Olivia A. De Meo[1], Fei Da[1], and Juliette L. Smith[1]

[1]Virginia Institute of Marine Science, William & Mary, Gloucester Point, VA, USA, [2]CSIRO Oceans and Atmosphere, Hobart, TAS, Australia, [3]Department of Meteorology and Atmospheric Science, The Pennsylvania State University, University Park, PA, USA

Key Points:
- An estuarine mass balance of dissolved inorganic carbon shows contributions from biological processes, circulation, and air-sea exchange
- Over a complete seasonal cycle, the mesohaline and polyhaline regions of the mainstem Chesapeake Bay act as a net sink of atmospheric CO_2
- A spatial gradient throughout the mainstem shows the largest net community production and sink of atmospheric CO_2 in mesohaline regions

Correspondence to:
E. H. Shadwick,
Elizabeth.shadwick@csiro.au

Citation:
Friedman, J. R., Shadwick, E. H., Friedrichs, M. A. M., Najjar, R. G., De Meo, O. A., Da, F., & Smith, J. L. (2020). Seasonal variability of the CO_2 system in a large coastal plain estuary. *Journal of Geophysical Research: Oceans*, *125*, e2019JC015609. https://doi.org/10.1029/2019JC015609

Received 4 SEP 2019
Accepted 2 JAN 2020
Accepted article online 16 JAN 2020

Abstract The Chesapeake Bay, a large coastal plain estuary, has been studied extensively in terms of its water quality, and yet, comparatively less is known about its carbonate system. Here we present discrete observations of dissolved inorganic carbon (DIC) and total alkalinity from four seasonal cruises in 2016–2017. These new observations are used to characterize the regional CO_2 system and to construct a DIC budget of the mainstem. In all seasons, elevated DIC concentrations were observed at the mouth of the bay associated with inflowing Atlantic Ocean waters, while minimum concentrations of DIC were associated with fresher waters at the head of the bay. Significant spatial variability of the partial pressure of CO_2 was observed throughout the mainstem, with net uptake of atmospheric CO_2 during each season in the upper mainstem and weak seasonal outgassing of CO_2 near the outflow to the Atlantic Ocean. During the time frame of this study, the Chesapeake Bay mainstem was (1) net autotrophic in the mixed layer (net community production of 0.31-mol C m^{-2}·$year^{-1}$) and net heterotrophic throughout the water column (net community production of −0.48-mol C m^{-2}·$year^{-1}$), (2) a sink of 0.38-mol C m^{-2}·$year^{-1}$ for atmospheric CO_2, and (3) significantly seasonally and spatially variable with respect to biologically driven changes in DIC.

Plain Language Summary Water quality in the Chesapeake Bay, the largest estuary in the continental United States, has been extensively monitored for over 30 years, yet relatively less is known about the cycling of carbon in these waters. The data collected in this study demonstrate considerable seasonal and spatial variability of dissolved carbon dioxide (CO_2) in the Chesapeake Bay mainstem. Much of this variability is driven by the physical setting: Waters have lower salinity in the northern Bay due to riverine inputs and higher salinity in the southern Bay due to exchange with the Atlantic Ocean. Changes in salinity driven by estuarine circulation patterns throughout the mainstem have a large influence on the seasonal and spatial variability of CO_2, as do biological processes. In surface waters of the mainstem, photosynthesis is greater than respiration over a complete seasonal cycle. In the years studied, there is also large spatial variability with respect to the uptake of atmospheric CO_2. Through the combination of changes in salinity and biological processes, the mainstem of the bay acts as a net sink of atmospheric CO_2.

1. Introduction

In the open ocean, the uptake of anthropogenic carbon dioxide (CO_2) has decreased the surface ocean pH by 0.1 standard units over the past century (Doney et al., 2009; Dore et al., 2009; Orr et al., 2005), but the impact of rising atmospheric CO_2 on estuarine water chemistry is less well understood (Sunda & Cai, 2012; Waldbusser & Salisbury, 2014). Coastal systems are influenced by additional anthropogenic stressors, such as urban development and atmospheric deposition of nitrogen from fossil fuel combustion and agricultural activities, that may have compensatory or additive effects on changes to the CO_2 system (Da et al., 2018; Doney, 2010; Sunda & Cai, 2012). Additionally, nearshore systems may experience greater seasonal and interannual variability than their open-ocean counterparts due to their sensitivity to changes in highly variable riverine discharge.

Recurring hypoxia in the deep channel of the Chesapeake Bay (CB) mainstem is stimulated by eutrophication and the resulting production and respiration of excess organic matter (Hagy et al., 2004; Harding et al., 2014; Harding et al., 2016; Zimmerman & Canuel, 2000). If the organic matter generated by phytoplankton growth is not consumed locally or laterally exported from the region, it sinks and subsequent

remineralization consumes dissolved oxygen (O_2) and leads to elevated concentrations of dissolved inorganic carbon (DIC) at depth (e.g., Cai et al., 2004, 2011; Shen, Testa, Li, et al., 2019; Shen, Testa, Ni, et al., 2019). Reduced vertical exchange during periods of seasonal stratification prevents the ventilation of high-DIC and low-O_2 waters at depth and the accumulation of DIC at depth may exacerbate coastal acidification in eutrophic estuarine systems. The annual occurrence of low-O_2 and high-DIC concentrations in subsurface waters was documented in a summer study in the upper CB main stem by Cai et al. (2017) and has been reported in other coastal systems, including the Baltic Sea and the Gulf of Mexico (Hu et al., 2017; Schneider, 2011).

Estuaries encompass 4% of the global coastal ocean surface area and are generally characterized as heterotrophic systems that act as net sources of CO_2 to the atmosphere (Borges, 2005; Joesoef et al., 2015; Laruelle et al., 2010, 2015; Najjar et al., 2018). More specifically, it has been estimated that estuaries along the east coast of the United States release approximately 110 g C m^{-2}·$year^{-1}$ to the atmosphere (Najjar et al., 2018). Here we present new observations spanning four seasons (Autumn 2016 to Summer 2017) to diagnose the spatiotemporal variability of the CO_2 system in the main stem of the CB, the largest estuary in the continental United States. This study builds on a growing body of work focused on the seasonality of the CO_2 system in the region (e.g., Brodeur et al., 2019; Shadwick, Friedrichs, et al., 2019; Shen, Testa, Li, et al., 2019). New shipboard observations are used to partition the seasonality of DIC into physical and biological drivers. This quantitative separation of processes yields estimates of net community production for the surface layer and the waters below the mixed layer and an annual assessment of the air-sea exchange of CO_2 in four regions within the CB mainstem.

2. Methods

2.1. Data Collection and Analysis

The CB Water Quality Monitoring Program (CBMP; Chesapeake Bay Program, 2012, https://www.chesapeakebay.net) samples the mainstem monthly in the cooler months and twice monthly in the warmer months (May–September). The Maryland (MD) portion of the CB mainstem is monitored by the Maryland Department of Natural Resources (MD DNR), while the Virginia (VA) portion is monitored by the Virginia Department of Environmental Quality (VA DEQ), in collaboration with Old Dominion University (ODU). Discrete samples of DIC and total alkalinity (TA) were collected at 17 stations (Figure 1, Table 1) on four CBMP cruises from 2016 to 2017: autumn (14 to 16 November, 2016), winter (14 to 17 February, 2017), spring (8 to 11 May, 2017), and summer (10 to 17 July, 2017). The maximum depth of each station ranged from 4 to 32 m.

At each station, samples were collected 1 m below the surface and 1 m above the bottom, as well as at two intermediate depths depending on station depth and depth of the mixed layer. Density profiles were computed at each station as a function of temperature, salinity (S), and pressure measured by the CBMP. The mixed-layer depth (MLD) was estimated using a percentage threshold, where stratification is assumed to occur if there is a change on the order of 10% of the difference between the maximum and minimum values of the density profile observed within 1 m (Irby et al., 2016). Therefore, the MLD is defined as the shallowest occurrence (below 1m depth) where this percentage threshold is observed.

Onboard the MD DNR vessel, the R/V Kerhin, discrete samples were collected using a Dayton 10 GPM submerged well pump. In VA waters, samples were collected using a SeaBird 32 Mini-rosette with 12.5-L Ocean Test Equipment Go-Flo bottles onboard the ODU vessel, R/V Fay Slover. In both regions, a YSI 6820 was used to measure temperature, S, O_2, and pH at 1 to 2m resolution depending on station depth. From herein, pH measured by the CBMP sensors will be referred to as pH_{MP} to distinguish it from pH calculated using methods described below.

Samples were collected in 250ml borosilicate bottles for the quantification of DIC and TA. Samples collected in VA were fixed using a saturated solution of mercuric chloride ($HgCl_2$) immediately after collection, then stored in the dark to await analysis. Samples collected in MD were immediately stored on ice in the dark and poisoned 2–6 hr after collection as $HgCl_2$ was not permitted onboard the R/V Kerhin. All samples were returned to the Virginia Institute of Marine Science (VIMS) for laboratory analysis. Concentrations of DIC and TA were measured using a nondispersive infrared analyzer, Automated Infrared Inorganic Carbon

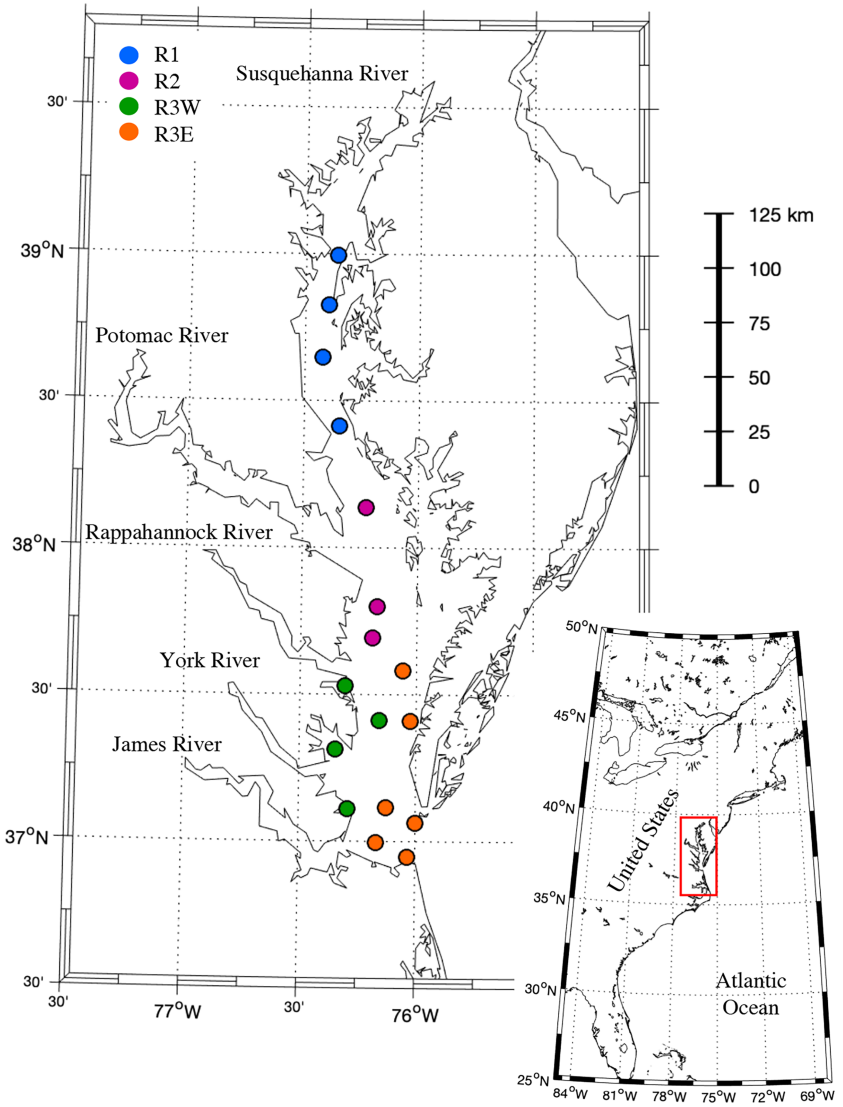

Figure 1. Regional partitioning of the study area: R1 (blue), R2 (magenta), R3E (orange), and R3W (green), with major rivers indicated.

Analyzer (AIRICA, Marianda), and an open-cell potentiometric titrator (components from Metrohm), respectively. Analysis of Certified Reference Materials (provided by A. G. Dickson, Scripps Institute of Oceanography; Batch #150 for autumn, winter, and spring and Batch #166 for summer) ensured an uncertainty of DIC and TA on the order of 2 and 3 $\mu mol \cdot kg^{-1}$, respectively. To quantify the impact of delayed $HgCl_2$ addition in MD samples, duplicate samples were collected in VA. Of the duplicates, one was treated with $HgCl_2$ immediately, and the other was stored on ice and treated after 6 hr. The difference in DIC concentrations between duplicate samples was indistinguishable from the analytical uncertainty. It is possible that the addition of $HgCl_2$ may induce reactions that affect alkalinity in low-salinity, hypoxic, water (Hiscock & Millero, 2006). However, because most of our samples were more saline than the $S < 5$ threshold and the relationship between TA and salinity derived from observations is similar to that Brodeur et al. (2019) who did not fix TA samples with $HgCl_2$ at low salinity, we assume the impact on our TA concentrations is not significant. Following the determination of DIC and TA, the CO2SYS program (van Heuven et al., 2011) was used to compute pH (on the total scale) and the partial pressure of CO_2 (pCO_2). Silicate and phosphate measured by the CBMP (Chesapeake Bay Program, 2012) were used along with the equilibrium constants of Mehrbach et al. (1973) refit by Dickson and Millero (1987) and the KSO_4 constant of Dickson (1990).

Table 1
Depth and Location of Each Station Used in This Analysis

Station	Region	Latitude (°N)	Longitude (°W)	Station Depth (m)
CB3.3C	R1	38.996	−76.360	24
CB4.1C	R1	38.826	−76.400	32
CB4.2C	R1	38.646	−76.421	27
CB4.4	R1	38.415	−76.346	31
CB5.2	R2	38.137	−76.228	31
CB5.4	R2	37.800	−76.175	32
CB5.5	R2	37.692	−76.190	17
CB6.3	R3W	37.412	−76.160	11
LE3.7	R3W	37.531	−76.307	6
WE4.1	R3W	37.312	−76.346	4
WE4.4	R3W	37.110	−76.293	4
CB7.1S	R3E	37.581	−76.058	16
CB7.2E	R3E	37.412	−76.025	12
CB7.3	R3E	37.117	−76.125	12
CB7.4N	R3E	37.062	−75.999	10
CB8.1	R3E	36.995	−76.168	8
CB8.1E	R3E	36.947	−76.035	14

2.2. Assignment of Geographic Regions

To reflect the natural, spatial variability in hydrographic and biogeochemical parameters throughout the CB, the mainstem was divided into four regions (Figure 1) based on surface salinity. The northern region, Region 1 (R1), encompasses the deep oligohaline (S = 0.5–5) portion of the mainstem channel, where seasonal stratification was present after large freshwater inputs in the spring and summer. Region 2 (R2) is unique as its salinity regime shifts seasonally from mesohaline in the spring and summer (S = 5–18) to polyhaline (S > 18) in autumn and winter. Maximum station depth in both R1 and R2 was 32 m. Within R2, sampling was biased towards the deep channel in the western portion of the region. The most southern region was divided longitudinally due to the circulation pattern in the lower CB. As more saline ocean waters enter the mouth of the CB, they flow north along the Eastern Shore of VA where the mainstem is deeper and has decreased freshwater inputs (R3E; Goodrich & Blumberg, 1991). In this region, maximum station depth was 16 m. Stations in the western half of the lower CB (R3W) receive greater freshwater inputs from the James, York, and Rappahannock Rivers with a maximum station depth of 11 m. We assume that the observations used here are representative of each region (Table 2) yet recognize that the uneven spatial distribution of stations will result in uncertainty in measured and derived parameters in each region.

2.3. Estimate of Total Alkalinity During the Winter Season

DIC and TA samples were collected during the winter season in the upper CB, but were not collected from the VA portion of the CB during the February (winter) cruise. We used the following procedure to estimate the missing winter values: First, a relationship between TA and salinity was derived using all available measurements of TA from samples collected by VIMS between June 2016 and January 2018 (Figure 2a). Additional observations outside seasons included in this analysis are used to generate the most robust relationship between TA and S (Shadwick, De Meo, et al., 2019). Second, winter TA values were computed with (see Figure 2a)

$$TA_{winter} = 38.6\,S + 978.2, \quad (1)$$

where TA_{winter} is the computed TA concentration in units of $\mu mol \cdot kg^{-1}$ at a given salinity. Finally, winter DIC and pCO_2 were computed using CO2SYS with TA_{winter} and pH_{MP} as described above. We note that the water quality pH_{MP} are not of the same quality as pH = f(DIC, TA), and the use of these data will add uncertainty to the resulting estimates of DIC and pCO_2. To better constrain this uncertainty, pCO_2 computed on the basis of DIC and TA in the autumn season minus pCO_2 computed on the basis of TA and pH_{MP} was calculated. The resulting mean of this difference was −32 μatm, and the standard deviation of this difference was 28 μatm.

2.4. Air-Sea CO_2 Flux

Table 2
Wind Speed in Each Region and Season, in $m \cdot s^{-1}$, Used to Calculate Air-Sea CO_2 Fluxes

Region	Autumn	Winter	Spring	Summer	Surface area
R1	5.6	5.5	4.4	5.3	908,849,967
R2	5.6	5.5	4.7	5.1	1,474,652,418
R3W	6.2	4.2	5.8	5.1	949,566,911
R3E	6.2	4.2	5.8	5.1	1,727,035,455

Note. Regional surface areas provided in m^2 and determined from Chesapeake Bay Program (2004).

The air-sea CO_2 flux (F) was computed using

$$F = k \cdot a \cdot \Delta pCO_2, \quad (2)$$

where k is the gas transfer velocity calculated using the formulation of Wanninkhof (2014) for intermediate wind speeds (3–15 $m \cdot s^{-1}$), a is the solubility coefficient of CO_2 (Weiss, 1974), and ΔpCO_2 is the gradient of CO_2 between the ocean and the atmosphere ($\Delta pCO_2 = pCO_2^{ocean} - pCO_2^{air}$). The flux is given in units of mol C $m^{-2} \cdot mon^{-1}$. When F is negative, there is an uptake of CO_2 by the surface waters. Wind speeds at a height of 4 m above the water surface were obtained from three buoys in the CB Interpretive Buoy System (CBIBS; https://buoybay.noaa.gov): the Gooses Reef Buoy for R1, the Potomac Buoy for R2, and the York

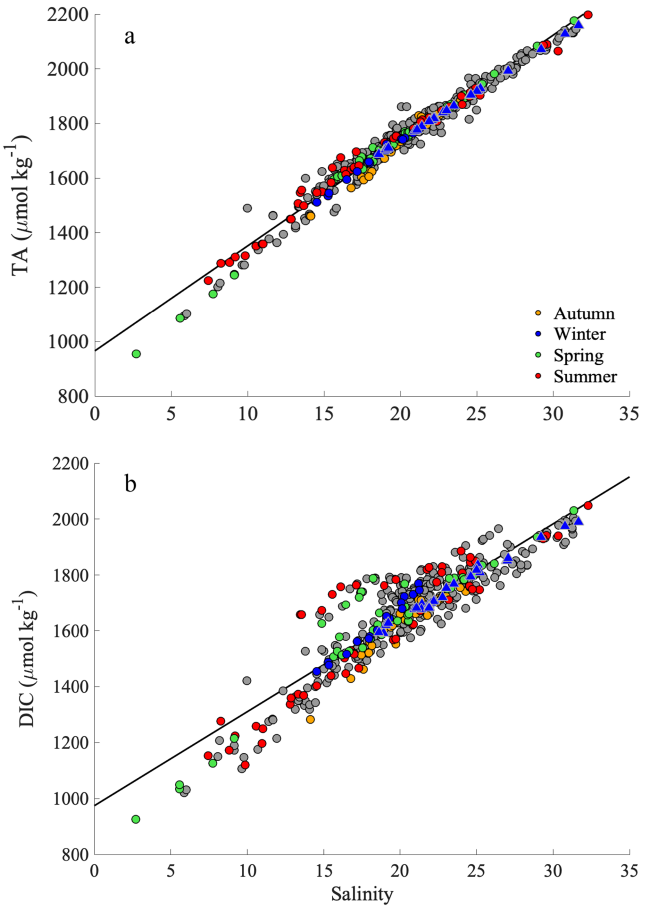

Figure 2. The relationship between TA, DIC, and salinity in the CB mainstem based on all samples collected by VIMS between June 2016 and January 2018 throughout the water column. Seasons used in this analysis are shown by the colored points. Linear regression analysis based on circle symbols yielded the following equation (black line): (a) TA = 39.6 S + 966.6 (n = 505, R^2 = 0.96, p < 0.001, SE = 7 μmol·kg^{-1}, uncertainty associated with the slope and intercept are 0.2 units in salinity, and 4 μmol·kg^{-1}, respectively); TA_{winter} values computed from this relationship are shown in blue triangles and (b) DIC_{sal} = 34.6 S + 973.2 (n = 505, R^2 = 0.87, p < 0.001, SE = 12 μmol·kg^{-1}, uncertainty associated with the slope and intercept are 0.3 units in salinity, and 7 μmol kg^{-1}, respectively). The winter values from VA (i.e., $DIC_{winter} = f(TA_{winter}, pH_{MP})$) are shown in blue triangles.

Spit Buoy for R3E and R3W. The York Spit Buoy is located in R3W, but the wind speed from this location was used for R3E as well due to an incomplete record of wind speed in R3E for the period of observation. The average wind speed over each cruise was used (i.e., spring cruise was 4 days; Table 2). The atmospheric CO_2 used in this study is the 2016 average, 405.6 μatm, from the World Data Center for Greenhouse Gases station in Key Biscayne, Florida. As we show below, the surface water pCO_2 varies by almost 300 μatm, which is much larger than the atmospheric pCO_2 (seasonal range ~10 μatm), and hence, we assume air-sea fluxes are relatively insensitive to the use of a single mean atmospheric pCO_2 value. The regional fluxes were found by computing the flux at each station in each region (Table 3) then averaging over all the stations in a region. These regional fluxes were then scaled to the surface area of each region. The surface areas of each region were determined using Chesapeake Bay Program (2004) segment CB4MH, encompassing the northern deep channel of R1, segment CB5MH corresponding to the western middle bay where samples were collected in R2, segment CB6PH and half of CB8PH corresponding to R3W, and segment CB7PH and half of CB8PH encompassing the surface area of R3E. The sum of the area-weighted fluxes in each season were used to determine the annual source/sink status of atmospheric CO_2 in the CB main stem.

2.5. Mass Balance of DIC

The total change in DIC concentration per unit time (ΔDIC_{total}) is equal to the sum of the changes due to biological drivers—photosynthesis, respiration, and biogenic calcification (ΔDIC_{bio})—and physical drivers—air-sea CO_2 exchange (ΔDIC_{gas}), horizontal and vertical mixing, or circulation (ΔDIC_{circ}), and calcium carbonate ($CaCO_3$) dissolution. Due to the conservative behavior of TA as a function of salinity (equation (1)), we assume that calcification and dissolution of $CaCO_3$ are negligible (Figure 2a). In the mixed layer, the change in DIC between seasons (in units of μmol·kg^{-1}·month^{-1}) can thus be expressed as

$$\Delta DIC_{total}{}^{ML} = \Delta DIC_{bio}{}^{ML} + \Delta DIC_{circ}{}^{ML} + \Delta DIC_{gas}{}^{ML}. \quad (3)$$

In subsurface waters, the seasonal changes in DIC can be expressed as

$$\Delta DIC_{total}{}^{sub} = \Delta DIC_{bio}{}^{sub} + \Delta DIC_{circ}{}^{sub}. \quad (4)$$

$DIC_{total}{}^{ML}$ and $DIC_{total}{}^{sub}$ were computed by first determining the average concentration of DIC in the mixed layer and subsurface waters, respectively, (in units of μmol·kg^{-1}). The depth of the subsurface layer was determined at each station by subtracting the depth of the mixed layer (Table 3) from the total depth of the water column (Table 1). Both mixed layer and subsurface values were computed by averaging all of the values falling in each layer of the water column during a season in each region. $\Delta DIC_{total}{}^{ML}$ and $\Delta DIC_{total}{}^{sub}$ were computed as the difference of the mean DIC concentrations above and below the mixed layer, respectively, divided by the time in months between seasons. The change in time (Δt) between autumn and winter (i.e., the number of months between cruises), and winter and spring, was 3 months, and Δt between spring and summer was 2 months. $\Delta DIC_{gas}{}^{ML}$ was computed by taking the average of the air-sea CO_2 fluxes scaled by the average mixed layer depth between seasons in each region (Table 3). The impact of circulation was quantified by assuming that salinity is conservative and that there is, at any one time and place, a linear relationship between salinity and DIC. Because advection and diffusion, here referred to together as circulation, are linear processes (i.e., they are proportional to concentration and its derivatives, not higher order functions of the concentration), the use of a salinity-DIC relationship (given below) is a valid means for estimating DIC transport. The shortcoming of the approach is that there is

Table 3
Mean Values of Mixed Layer CO_2 System Parameters in Each Region

Parameter	DIC^{ML}	TA^{ML}	pH^{ML}	pCO_2^{ML}	S^{ML}	T^{ML}	MLD	*n*
Units	$\mu mol \cdot kg^{-1}$	$\mu mol \cdot kg^{-1}$		µatm		°C	m	
R1								
Autumn	1,364 ± 95	1,520 ± 69	8.50 ± 0.14	169 ± 59	16.2 ± 1.8	13.5 ± 0.4	3.3 ± 1.5	3
Winter	1,484 ± 26	1,547 ± 35	8.26 ± 0.05	245 ± 22	15.5 ± 1.0	4.8 ± 0.3	7.3 ± 3.8	3
Spring	1,033 ± 82	1,076 ± 91	8.28 ± 0.04	229 ± 26	5.3 ± 2.5	17.2 ± 0.4	5 ± 2.6	3
Summer	1,196 ± 51	1,316 ± 48	8.36 ± 0.14	193 ± 82	9.3 ± 1.5	27.1 ± 0.4	9.3 ± 2.9	4
R2								
Autumn	1,633 ± 7	1,753 ± 13	8.23 ± 0.01	307 ± 9	20.0 ± 0.5	13.7 ± 0.1	4.5 ± 0.7	2
Winter	1,585 ± 12	1,682 ± 21	8.32 ± 0.03	232 ± 34	18.5 ± 0.5	5.5 ± 0.2	3 ± 1.4	3
Spring	1,515 ± 10	1,611 ± 16	8.20 ± 0.01	343 ± 14	15.9 ± 0.4	17.2 ± 0.1	9 ± 5.7	2
Summer	1,384 ± 39	1,517 ± 50	8.26 ± 0.01	304 ± 3	13.6 ± 0.9	28.0 ± 1.2	7 ± 2.6	3
R3W								
Autumn	1,686 ± 44	1,808 ± 51	8.21 ± 0.01	326 ± 19	21.4 ± 1.5	13.5 ± 0.9	6 ±2.8	4
Winter	1,672 ± 37	1,780 ± 51	8.28 ± 0.03	256 ± 40	21.1 ± 1.4	6.0 ± 0.5	3.8 ±1.7	4
Spring	1,605 ± 43	1,718 ± 51	8.17 ± 0.02	381 ± 21	19.3 ± 1.5	18.5 ± 0.4	4.5 ± 2.1	4
Summer	1,575 ± 74	1,718 ± 81	8.14 ± 0.07	444 ± 85	18.6 ± 2.4	28.7 ± 0.3	4.3 ± 0.5	4
R3E								
Autumn	1,698 ± 61	1,852 ± 58	8.26 ± 0.05	289 ± 35	23.0 ± 1.8	14.4 ± 0.2	7 ± 5.7	2
Winter	1,801 ± 98	1,911 ± 119	8.20 ± 0.03	325 ± 56	24.8 ± 3.3	6.6 ± 0.5	3.8 ± 2.8	6
Spring	1,742 ± 72	1,861 ± 83	8.11 ± 0.02	434 ± 23	23.0 ± 2.2	17.6 ± 0.4	6.8 ± 2.6	6
Summer	1,623 ± 128	1,786 ± 120	8.16 ± 0.09	416 ± 103	21.2 ± 3.6	27.3 ± 1.9	3.7 ± 1.8	6

Note. The ± represents the standard deviation of the seasonal average of each parameter in each region; *n* is the number of stations included in the average. Abbreviations: DIC = dissolved inorganic carbon; MLD = mixed-layer depth; TA = total alkalinity.

some scatter in the salinity-DIC relationship (Figure 2b); however, that scatter is exploited to estimate the error (see section 2.7). The relationship between DIC and salinity is derived using all samples collected between June 2016 and January 2018 (Shadwick, De Meo, et al., 2019, Figure 2b):

$$DIC_{sal} = 33.5\,S + 973.2, \tag{5}$$

where DIC_{sal} has units of $\mu mol \cdot kg^{-1}$. DIC_{sal} was computed at each station during all seasons. The change in the mean DIC_{sal} from all stations in a given region between seasons was then assumed equal to ΔDIC_{circ}^{ML} and ΔDIC_{circ}^{sub}, in the mixed layer and subsurface waters, respectively. Finally, the contribution from biological processes in the mixed layer (ΔDIC_{bio}^{ML}) and subsurface waters (ΔDIC_{bio}^{sub}) were computed by difference. In the mixed layer (equation (6)) and subsurface waters (equation (7)), the contributions from biological processes were defined as

$$\Delta DIC_{bio}^{ML} = \Delta DIC_{total}^{ML} - \Delta DIC_{circ}^{ML} - \Delta DIC_{gas}^{ML}, \tag{6}$$

$$\Delta DIC_{bio}^{sub} = \Delta DIC_{total}^{sub} - \Delta DIC_{circ}^{sub}. \tag{7}$$

In the northern CB regions (R1 and R2), all stations contain both mixed-layer and subsurface values in each season. In R3E, there are stations that are well mixed throughout the water column in certain seasons (e.g., winter), but stratified in other seasons (e.g., summer). In R3W, there are both stations that are well mixed in each season and stations that experience stratification. In R3W, the autumn, winter, and summer subsurface budgets are based on observations from a single station; the spring subsurface budget is based on observations from two stations. In R3E, the autumn subsurface budget is based on observations from a single station, as all other stations are well mixed and therefore included in the mixed layer budget. The sum of the mixed layer and subsurface values are used to generate whole water column values of ΔDIC_{bio} (ΔDIC_{bio}^{full}) and subsequently net community production. To convert from concentration of DIC ($\mu mol \cdot kg^{-1}$) in the mixed layer and subsurface waters to units of mol C $m^{-2} \cdot month^{-1}$, the average seasonal density in each region is needed, along with average depth of the mixed layer and subsurface layer in each region during each season.

2.6. Net Community Production

Net community production is defined as the difference between net primary production (NPP) and heterotrophic respiration (HR):

$$NCP = NPP - HR, \quad (8)$$

and it is equal to the net biologically driven changes of DIC (i.e., net community production [NCP] = $\Sigma\Delta DIC_{bio}$) resulting from the mass balance of DIC described above. The sum of the mixed layer and subsurface values are used to generate whole water column values of ΔDIC_{bio} and subsequently NCP. To convert from concentration of DIC ($\mu mol \cdot kg^{-1}$) to units of mol C m^{-2} $month^{-1}$, the average seasonal density in each region is needed, along with the average depth of the mixed layer and subsurface layer in each region during each season. Recall that observations were collected from November 2016 to July 2017; we therefore define an annual cycle as autumn-winter-spring-summer. Because we did not sample in autumn 2017, and because interannual variability in net community production in the region is known to be large (e.g., Feng et al., 2015), we do not compute the difference between summer 2017 and the previous autumn to close the annual cycle and instead assume that there was no change in DIC_{bio} between summer 2017 and autumn 2017, a season which we did not sample, to scale our estimate of NCP over a full year.

2.7. Uncertainty Analysis

Because ΔDIC_{bio} was computed by difference, the uncertainty of this term includes the uncertainty associated with each of the other terms in equations (5) and (6). The uncertainty associated with ΔDIC_{total} was small (2 $\mu mol \cdot kg^{-1}$) and based on the analytical uncertainty of the measurement. The uncertainty associated with ΔDIC_{gas}^{ML} was estimated from the standard deviation of the flux computed via three different parameterizations of the gas transfer velocity—Wanninkhof (2014), Wanninkhof and McGillis (1999), and Nightingale et al. (2000)—and was on the order of 5 $\mu mol \cdot kg^{-1}$, corresponding to 0.03 mol C $m^{-2} \cdot month^{-1}$ (assuming a mean mixed-layer depth of 5.4 m and a mean density of 1,013 $kg \cdot m^{-3}$). We note that uncertainty in the air-sea flux is also due to the use of an annual mean value of atmospheric CO_2, but, as noted in section 2.4, this uncertainty is small and not included. The uncertainty associated with ΔDIC_{circ} was estimated to be 12 $\mu mol \cdot kg^{-1}$, determined from the standard error of the regression between DIC and salinity (equation (5); Figure 2b). The resulting uncertainty associated with the ΔDIC_{bio} in the mixed layer (13 $\mu mol \cdot kg^{-1}$) and subsurface waters (12 $\mu mol \cdot kg^{-1}$) was computed by propagating the errors associated with all other terms (i.e., $(3^2 + 5^2 + 12^2)^{1/2}$ for the mixed layer) and assuming that the errors are uncorrelated.

3. Results

3.1. Representativeness of Mainstem Cruises

From the long-term (1984–2017) CBMP climatology in each region, it is clear that the four 2016/2017 cruises included in this analysis are representative of the broad hydrographic seasonality in the CB main stem, with few observed values outside the range of the long-term data (Figure 3). Furthermore, riverine discharge from the Susquehanna, Potomac, and James Rivers during the 2016/2017 year was normal with maximum discharge observed during the spring season; that is, the observations presented here were not collected in a particularly wet, or particularly dry year (United States Geological Survey, 2018). Throughout the CB main stem, waters exhibit a pronounced seasonality in surface temperature (SST; seasonal range on the order of 30 °C, Figures 3a, 3c, 3e, and 3g). Temperature in all four regions ranged from less than 5 °C in winter to greater than 25 °C in summer. Seasonality in salinity shows maximum values in winter and some degree of freshening in the spring and summer seasons across all regions (Figure 3b, 3d, 3f, and 3h).

3.2. CO_2 System Seasonality in the Mainstem

The seasonality of the CO_2 system is influenced by both hydrographic (i.e., changes in temperature and salinity) and biological (i.e., photosynthesis and respiration) drivers, as well as the air-sea exchange of CO_2, with different parameters exhibiting differing sensitivity to these changes. As stated above, temperature exhibits a pronounced seasonality in all regions both within and below the mixed layer (Figures 4a and 5a). Salinity reveals the expected seasonality in streamflow; there is a smaller seasonal change in southern regions of the main stem as a result of the reduced freshwater input to the lower CB (Figure 4b). This is particularly

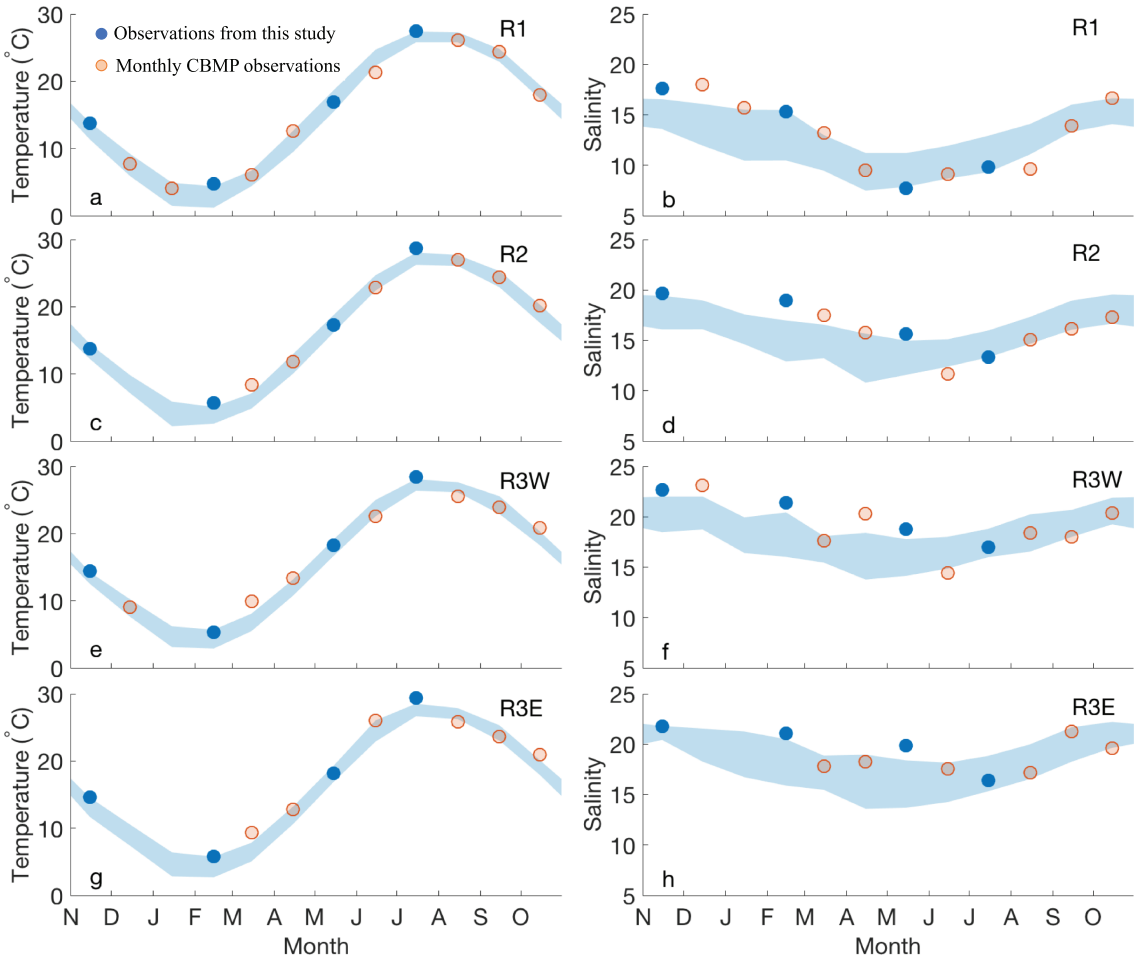

Figure 3. Climatological surface temperature (a, c, e, g) and salinity (b, d, f, h) from CBMP (data from 1984 to 2017), with shaded areas indicating the 25th and 75th percentiles. Seasonal temperature and salinity observations used in this analysis are shown in blue circles; orange circles indicate all other months observed over the study period. Temperature and salinity data from one station per region were used to illustrate the observed seasonality; (a and b) station CB4.2C in R1, (c and d) station CB5.4 in R2, (e and f) station CB6.3 in R3W, and (g and h) station CB7.1S in R3E.

evident in the mixed layer, where the regions with greatest freshwater input have the largest seasonality in salinity, while below the mixed layer the seasonality is reduced (Figure 5b). The seasonality of DIC and TA almost perfectly mimic that of salinity in each region both in and below the mixed layer (Tables 3 and 4; Figures 4a, 4b, and 4c). Minimum concentrations of DIC and TA (~1,000 μmol·kg^{-1} in the mixed layer, 1,500 μmol·kg^{-1} below) were observed in the northern CB. Maximum concentrations of DIC and TA were observed at the mouth of the CB, with mixed-layer maxima on the order of 1,800 μmol·kg^{-1} and 1,900 μmol·kg^{-1}, respectively, and subsurface maximum concentrations on the order of 1,900 μmol·kg^{-1} and 2,000 μmol·kg^{-1}, respectively (Figures 4c, 4d, 5c, and 5d). The seasonality in mixed-layer DIC and TA indicated pronounced minima in spring followed by a modest increase in summer in R1, while the other regions indicated a steadier decline from winter to summer. Below the mixed layer the seasonality was weaker, with a small increase in DIC and TA in spring in R1 and relatively steady concentrations in the other regions over all seasons (Figures 5c and 5d). The mixed-layer pH ranged from below 8.0 to 8.3 and was a minimum in summer in all regions, with the lowest values (<8.0) observed in R3E (Figure 4e). Below the mixed layer, the pH ranged from 8.1 to a minimum of 7.2 (in R1), with the lowest values observed in the summer season, and corresponding to the maximum SST, in all regions (Figure 5e). The seasonality in mixed-layer pCO_2 is large and ranged from a minimum of ~170 μatm to a maximum ~450 μatm with the lowest values corresponding to the autumn and summer seasons in R1 and the highest values corresponding to the spring and summer seasons in R3E and R3W. The supersaturation

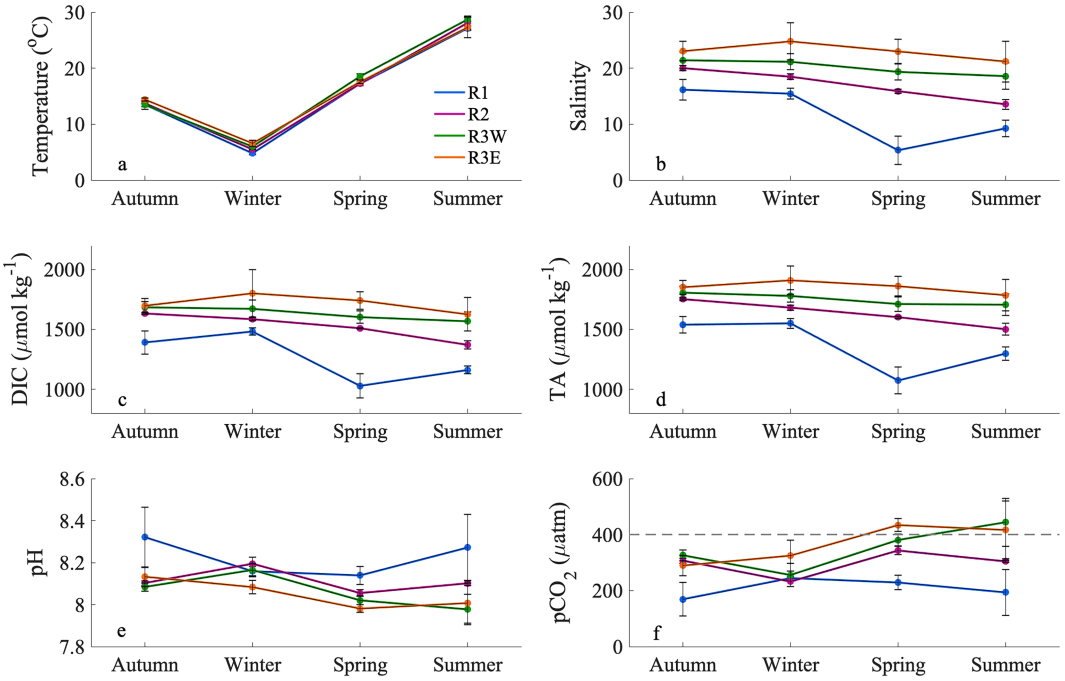

Figure 4. The seasonal cycle in the surface mixed layer of (a) temperature, (b) salinity, (c) DIC, (d) TA, (e) pH, (f) pCO_2 with regions distinguished by color. Values below the dashed line in (f) indicates the concentration of atmospheric CO_2 (406 μatm). Error bars represent one standard deviation and two standard deviations in the case of the winter pCO_2.

with respect to the atmosphere was coincident with the maximum surface temperature and was consistent with observations of CO_2 outgassing in other temperate systems during the productive season due to the dominance of warming in controlling the pCO_2 (e.g., the Scotian Shelf and Gulf of Maine, Shadwick et al., 2011; Vandemark et al., 2011). Below the mixed layer, the seasonal change in pCO_2 was even larger, with a maximum greater than 2,800 μatm in R1 in summer corresponding to the maximum temperature and consistent with the occurrence of hypoxia in the upper main stem due to the delivery of organic matter that was subsequently respired, consuming oxygen and producing CO_2 (e.g., Cai et al., 2011). Below the mixed layer, the lowest pCO_2 values (250 to 350 μatm) correspond to the cooler autumn and winter seasons in R3E and R3W where interaction with the coastal Atlantic Ocean is greatest and undersaturation with respect to the atmosphere occurs.

The mainstem is a sink for atmospheric CO_2 on the annual scale, with a net uptake of 0.38 mol C m^{-2}·$year^{-1}$. The largest fluxes are observed in R1 (Figure 6), are fairly consistent with season, and have an annual average of −0.32 mol C m^{-2}·$month^{-1}$. In R2, there is more variability throughout the year, with the maximum flux occurring in winter and the annual average of −0.19 mol C m^{-2}·$month^{-1}$ roughly 40% lower than in R1. In the lower bay, the fluxes are smaller in all seasons, with annual means of 0.06 and 0.04 mol C m^{-2}·$month^{-1}$ for R3W and R3E, respectively. Both regions in the lower bay exhibit weak outgassing in summer, and R3E exhibits weak outgassing in spring, but we note that these fluxes are not statistically distinguishable from zero, and the lower bay may be neutral (i.e., neither a source nor a sink for atmospheric CO_2) in these seasons (Figure 6).

3.3. Seasonal Mass Balance of DIC

Changes in circulation and biology were found to have similar importance with respect to seasonal changes in DIC throughout the main stem, in both the mixed layer and below (Table 5, Figures 7 and 8). In R1, mixed layer changes due to circulation dominate between winter and spring, and spring and summer, while biology dominates between autumn and winter. Gas exchange plays the largest role in R2, and during spring and summer, changes due to biology and circulation are of similar magnitude in R2 and R3E. The smallest mixed layer changes due to circulation and biology are found in R3W, which may be partly due to the near shore locations of the stations in this region (Figure 1). Considering the mixed layer of entire mainstem, changes

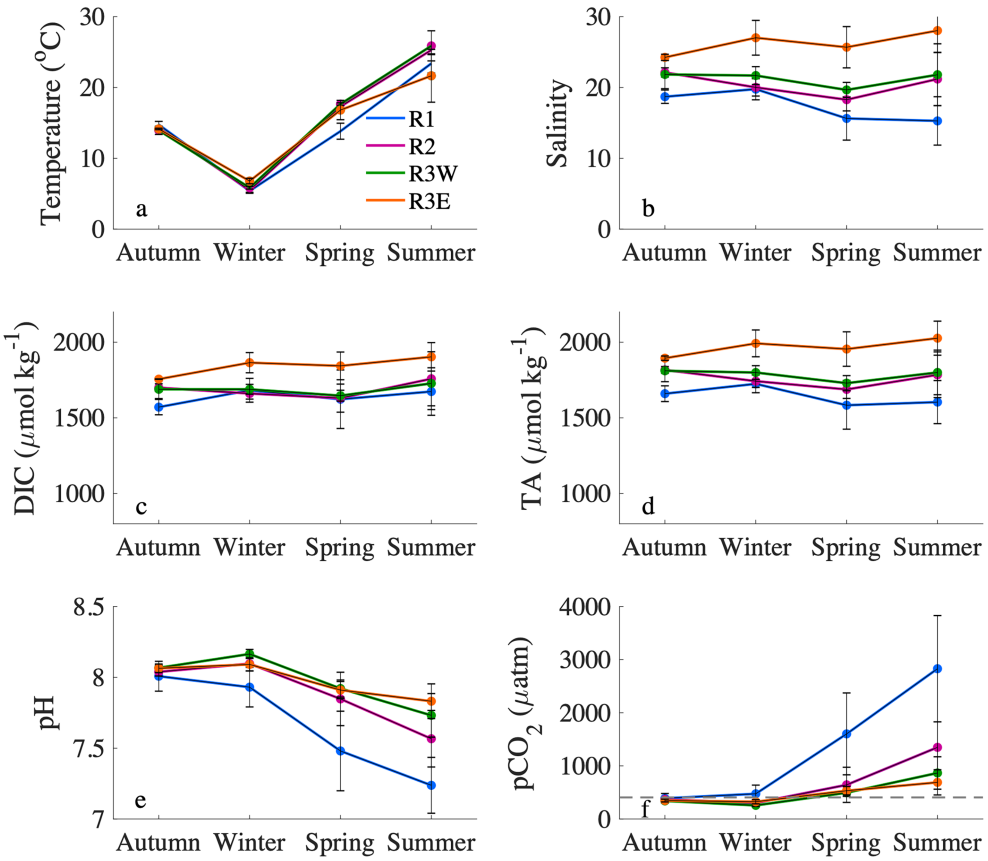

Figure 5. The seasonal cycle throughout the subsurface waters of (a) temperature, (b) salinity, (c) DIC, (d) TA, (e) pH, and (f) pCO_2 with regions distinguished by color. The dashed line in (f) indicates the concentration of atmospheric CO_2 (406 μatm). Error bars represent one standard deviation and two standard deviations in the case of the winter pCO_2.

due to circulation dominate between winter and spring, highlighting the importance of freshwater input in controlling DIC concentrations in the estuary. Biology acts to decrease DIC (photosynthesis) between winter and spring and spring and summer, with gas exchange partially offsetting this decrease. Respiration increases DIC between autumn and winter with a negligible contribution from circulation and an increase due to gas exchange of similar magnitude as the biological component.

Below the mixed layer, the biological control on DIC is positive in nearly all seasons and across all regions (Figure 8). The largest contributions from biology are in R1 and are of nearly constant magnitude over the year, indicating the expected dominance of respiration of organic material delivered from above. In R2 and R3W, biology is smaller than the contribution from circulation in all seasons, but as in R1 is positive indicating respiration or remineralization of organic matter below the mixed layer. In R3E, we compute a negative contribution from biology between spring and summer, which would indicate photosynthesis. However, if the uncertainty is considered, this term may be positive, reflecting the expected remineralization or more likely a near-neutral contribution from biology in this season. Considering the entire mainstem, below the mixed layer, changes due to circulation dominate in all seasons and are negative only in the winter to spring transition.

4. Discussion

4.1. CO_2 System Seasonality in the Context of Earlier Work

A recent study in the CB by Brodeur et al. (2019) observed latitudinal gradients in DIC and TA throughout the mainstem that are similar to our findings. We find good agreement with respect to the seasonal ranges in DIC and TA in the midbay (corresponding most closely R2 in this analysis) and lower bay (corresponding to

Table 4
Mean Values of Subsutablerface CO_2 System Parameters in Each Region

Parameter	DIC^{sub}	TA^{sub}	pH^{sub}	pCO_2^{sub}	S^{sub}	T^{sub}	n
Units	μmol·kg^{-1}	μmol·kg^{-1}		μatm		°C	
R1							
Autumn	1571 ± 51	1660 ± 52	8.0 ± 0.11	389 ± 92	18.7 ± 0.95	14.8 ± 0.46	3
Winter	1682 ± 79	1725 ± 58	7.93 ± 0.14	475 ± 163	19.8 ± 1.5	5.4 ± 0.33	3
Spring	1623 ± 193	1583 ± 158	7.48 ± 0.28	1602 ± 771	15.6 ± 3.1	13.8 ± 1.1	3
Summer	1674 ± 157	1604 ± 143	7.24 ± 0.20	2829 ± 1000	15.3 ± 3.4	23.4 ± 1.4	4
R2							
Autumn	1700 ± 25	1817 ± 23	8.04 ± 0.03	366 ± 28	22.1 ± 0.66	14.3 ± 0.20	2
Winter	1661 ± 37	1743 ± 42	8.10 ± 0.05	303 ± 80	20.0 ± 1.2	5.49 ± 0.29	3
Spring	1630 ± 93	1688 ± 59	7.85 ± 0.19	643 ± 331	18.2 ± 1.6	17.3 ± 0.47	2
Summer	1758 ± 178	1785 ± 151	7.57 ± 0.20	1349 ± 480	21.2 ± 3.7	25.3 ± 0.65	3
R3W							
Autumn	1689 ± 61	1811 ± 72	8.07 ± 0.02	340 ± 21	21.8 ± 2.0	14.0 ± 0.59	1
Winter	1689 ± 33	1800 ± 45	8.17 ± 0.03	256 ± 40	21.7 ± 1.3	5.85 ± 0.19	1
Spring	1647 ± 36	1729 ± 50	7.92 ± 0.06	485 ± 69	19.7 ± 1.1	17.7 ± 0.18	2
Summer	1728 ± 174	1800 ± 147	7.73 ± 0.15	866 ± 306	21.8 ± 4.4	25.9 ± 2.1	1
R3E							
Autumn	1756 ± 2	1894 ± 14	8.06 ± 0.03	347 ± 27	24.3 ± 0.45	14.1 ± 0.10	1
Winter	1865 ± 67	1992 ± 88	8.09 ± 0.05	325 ± 78	27.0 ± 2.5	6.79 ± 0.38	3
Spring	1843 ± 92	1955 ± 114	7.91 ± 0.06	532 ± 79	25.7 ± 2.9	16.8 ± 1.3	3
Summer	1903 ± 94	2027 ± 112	7.83 ± 0.1	690 ± 237	28.0 ± 3.1	21.7 ± 3.7	5

Note. The ± represents the standard deviation of the seasonal average of each parameter in each region; *n* is the number of stations included in the average. Abbreviations: DIC = dissolved inorganic carbon; TA = total alkalinity.

R3W and R3E) with the observations of Brodeur et al. (2019) in both the mixed layer and below. The pH comparison is complicated by inconsistency in units, but we note that our observations are in good agreement with respect to overall seasonality, with decreased pH with depth and distance from the Bay mouth. In terms of pCO_2, we compare our observations with a recent modeling study: Shen, Testa, Li, et al. (2019) found regions R1 and R2 of this study to be net sinks of atmospheric CO_2, whereas the lower CB was in a net-balanced condition, which is consistent with our findings for 2016/2017. We note that the annual air-sea CO_2 flux determined by Shen, Testa, Li, et al. (2019) included the tidal, freshwater region of upper CB, located north of R1 of this study, in their annual estimate. This upper bay region, while small in terms of surface area, is a strong source of CO_2 to the atmosphere.

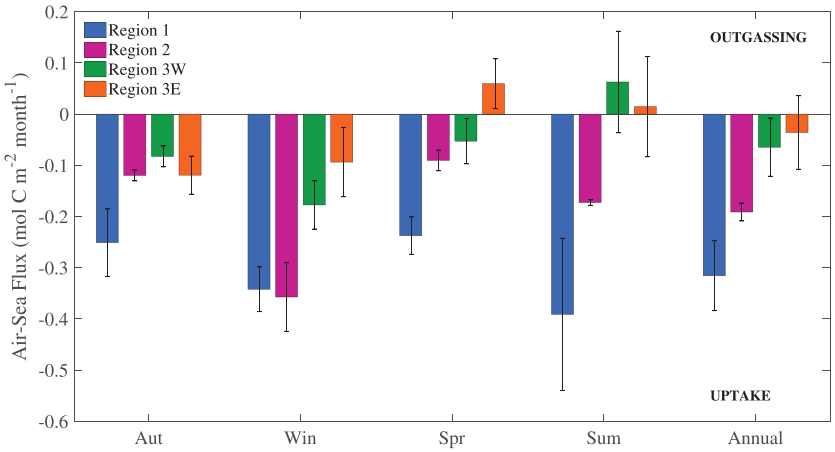

Figure 6. Air-sea CO_2 fluxes throughout the CB mainstem in all seasons and the annual average. Positive values indicate an outgassing of CO_2. Error bars represent one standard deviation and two standard deviations in the case of the winter values.

Table 5
Results of the DIC Mass Balance ($\mu mol \cdot kg^{-1} \cdot month^{-1}$) in the Mixed Layer and Whole Water Column

Parameter	ΔDIC_{total}^{ML}	ΔDIC_{gas}^{ML}	ΔDIC_{circ}^{ML}	ΔDIC_{bio}^{ML}	$\Delta DIC_{total}^{full}$	ΔDIC_{circ}^{full}	ΔDIC_{bio}^{full}
R1							
Autumn to winter	40	9	−3	34	77	9	13
Winter to spring	−150	8	−113	−45	−160	−133	−65
Spring to summer	81	7	72	2	106	66	−25
R2							
Autumn to winter	−16	12	−17	−11	−29	−41	−48
Winter to spring	−23	6	−26	−4	−54	−85	16
Spring to summer	−66	3	−37	−32	−2	12	−43
R3W							
Autumn to winter	−5	6	−4	−7	−5	−6	−37
Winter to spring	−22	6	−19	−9	−36	−42	−5
Spring to summer	−14	0	−9	−5	26	27	12
R3E							
Autumn to winter	35	4	20	11	70	51	2
Winter to spring	−20	1	−20	−1	−27	−35	19
Spring to summer	−58	−1	−31	−26	−28	8	−33

Abbreviation: DIC = dissolved inorganic carbon.

The neighboring Delaware Bay has a similar latitudinal gradient in salinity to that of the CB, and recent studies have characterized Delaware Bay as net heterotrophic and a source of atmospheric CO_2 on the annual scale (Joesoef et al., 2015, 2017). Unlike the CB, the Delaware Bay does not experience the impacts of eutrophication due to a lack of seasonal stratification (Sharp et al., 1982); the phytoplankton growth that is initiated after the introduction of excess nutrients to the upper CB contributes to maintaining pCO_2 undersaturation and the sink for atmospheric CO_2. More broadly, Najjar et al. (2018) showed that outgassing generally increases from Gulf of Maine estuaries (35 ± 9-g C $m^{-2} \cdot year^{-1}$) to mid-Atlantic Bight estuaries (52 ± 46 g C $m^{-2} \cdot year^{-1}$) to South Atlantic Bight estuaries (246 ± 117 g C $m^{-2} \cdot year^{-1}$). Our results indicate that CB uptake of atmospheric CO_2 (4.5 ± 1.2 g C $m^{-2} \cdot year^{-1}$) is an exception to this latitudinal gradient.

4.2. Net Community Production in the Context of Earlier Estimates

Between November 2016 and July 2017, the mixed layer of all regions in the CB is net autotrophic (i.e., $\Delta DIC_{bio}^{ML} < 0$; Table 6) indicating that net primary production dominated heterotrophic respiration and resulted in an overall net biological consumption of DIC (Table 5). The sum of the seasonal mixed layer NCP from each region (Table 6) scaled to the region's surface area (Table 2) results in a main stem NCP of 0.31 ± 0.1 mol C $m^{-2} \cdot year^{-1}$ with the error estimated from the uncertainty of the ΔDIC_{bio} terms (see section 2.7). When considering the whole water column, the mainstem had an NCP of −0.48 mol C $m^{-2} \cdot year^{-1}$, indicating net heterotrophic conditions (i.e., heterotrophic respiration > net primary production) during 2016/2017.

Kemp et al. (1997) estimated NCP in the main stem Bay using oxygen incubations and mass balance calculations based on carbon and nitrogen. These authors found distinct patterns in mainstem NCP that differ from the spatial variability presented here. The regional division of the CB mainstem used by Kemp et al. (1997) is different from this study; their midbay corresponds to R1 and R2, and their lower bay corresponds to our R3W and R3E, similar to the regional partitioning of Brodeur et al. (2019) described above. The tidal freshwater region used by Kemp et al. (1997) encompassed the low-salinity and high-turbidity zone near the mouth of the Susquehanna River and is not included in this study. This region, as well as the upper regions of CB tributaries, is often heterotrophic (e.g., Raymond et al., 2000) as a result of light limitation for primary production (Reay, 2009; Sin et al., 1999) and large amounts of bacterial respiration (Schultz, 1999). The inclusion of these low-light, high-turbidity zones in the upper CB of Kemp et al. (1997) contributes to their net heterotrophic findings in this region. The mid-CB of both Kemp et al. (1997) and the corresponding area of the mainstem mixed layer in this study (R1 and R2) were net autotrophic, whereas the whole water column of these regions was net heterotrophic. The annual NCP computed by Kemp et al. (1997) for this region was 13.6 ± 2.5 g C $m^{-2} \cdot year^{-1}$; the sum of the values of the complete seasonal cycle in the mixed layer of R1

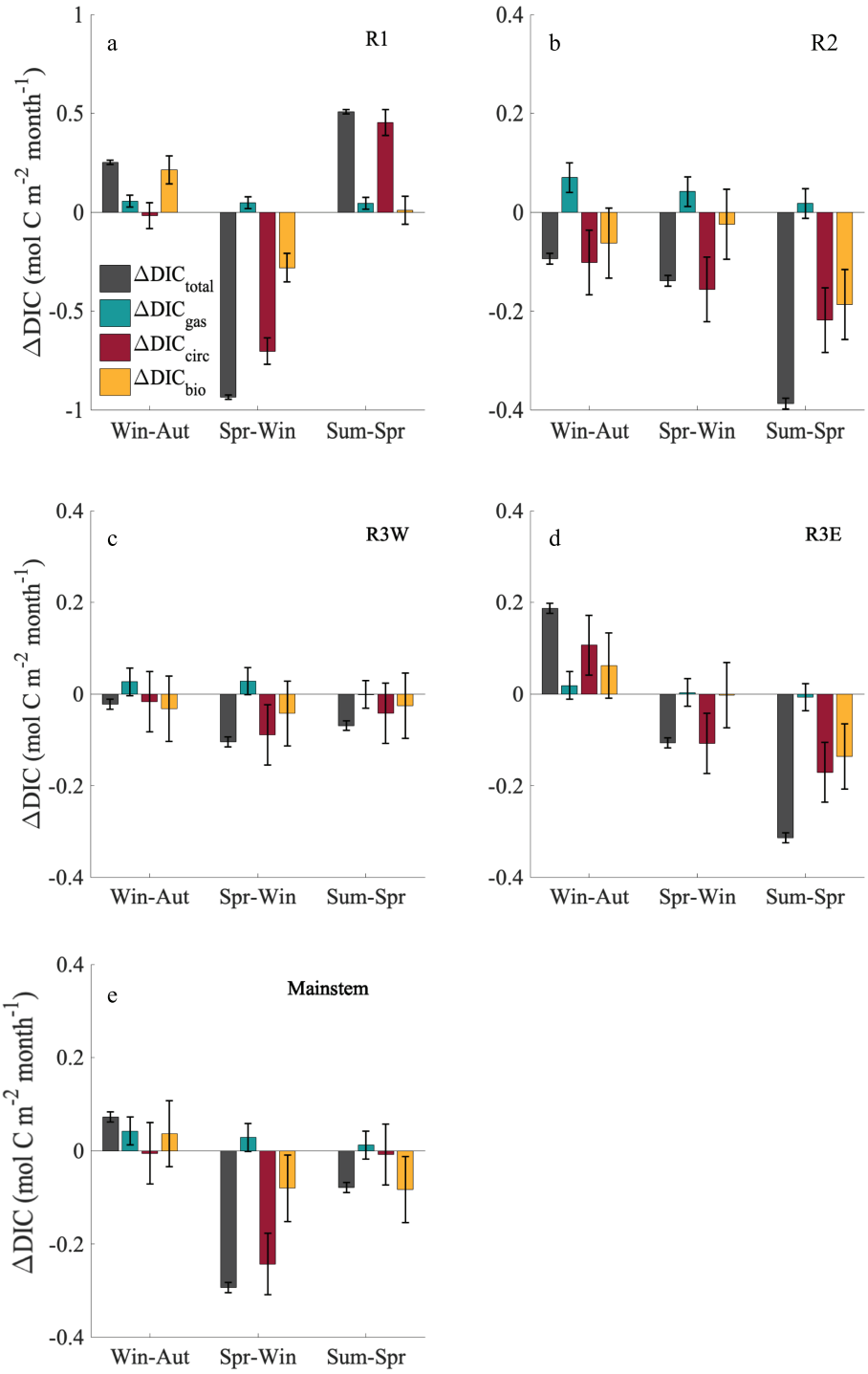

Figure 7. Terms in the mass balance of mixed layer DIC presented as differences between seasons (i.e., winter minus autumn is "Win-Aut"): total (gray), gas exchange (blue), circulation (red), and biology (yellow) in (a) R1; (b) R2; (c) R3W, (d) R3E, and (e) the seasonal average for the entire mainstem. Note the change of scale on the y-axes between regions R1 (a), and the remainder of the panels (b–e). Error bars indicate the estimated uncertainty for each term: 0.01 mol C m^{-2}·$month^{-1}$ for DIC_{obs}^{ML}, 0.03 mol C m^{-2}·$month^{-1}$ for DIC_{gas}^{ML}, 0.07 mol C m^{-2}·$month^{-1}$ for DIC_{circ}^{ML}, and 0.08 mol C m^{-2}·$month^{-1}$ for DIC_{bio}^{ML} (see section 2.6).

and R2 compare well with that of Kemp et al. (1997), at 10.0 ± 1.2 g C m^{-2}·$year^{-1}$, whereas the whole water column in this study had an annual value NCP −23.3 ± 1.2 g C m^{-2}·$year^{-1}$ (Table 6). In contrast to the results of Kemp et al. (1997), who determined that the lower CB (R3W and R3E) was net autotrophic, we

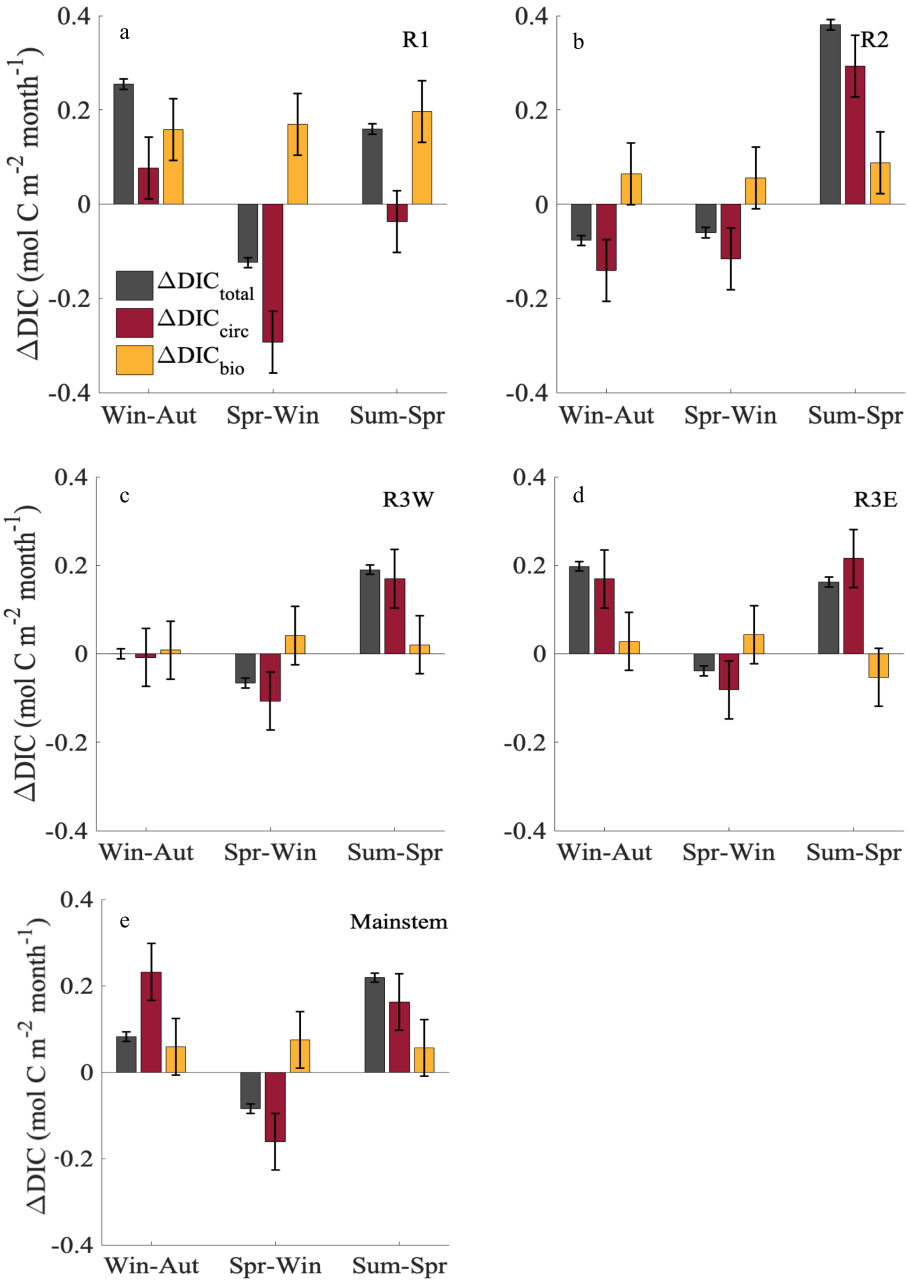

Figure 8. Terms in the mass balance of subsurface DIC presented as differences between seasons (i.e., winter minus autumn is "Win-Aut"): total (gray), circulation (red), and biology (yellow) in (a) R1; (b) R2; (c) R3W, (d) R3E, and (e) the seasonal average for the entire mainstem. Error bars indicate the estimated uncertainty for each term: 0.01 mol C m^{-2}·$month^{-1}$ for DIC_{obs}^{sub}, 0.07 mol C m^{-2}·$month^{-1}$ for DIC_{circ}^{sub}, and 0.07 mol C m^{-2}·$month^{-1}$ for DIC_{bio}^{sub} (see section 2.6).

found that the whole water column in the lower CB was net heterotrophic. This difference may be partly due to the inclusion of shallow stations in the lower bay of this study, particularly in R3W, compared to those used by Kemp et al. (1997). Part of the difference may also be a reduction in the delivery of nutrients to support primary production since the time period corresponding to the Kemp et al. (1997) analysis (data were collected from 1986 to 1993).

The 3-D hydrodynamic-biogeochemical modeling study of Feng et al. (2015) found the CB to be net autotrophic. If we convert their NCP values to carbon units using a Redfield ratio of C:N = 106:16, the authors' annual average for 2001–2005 is $4.2 \times 10^{11} \pm 1.3 \times 10^{11}$ g C $year^{-1}$. This is larger than our mixed layer

Table 6
Monthly (mol C m^{-2}·$month^{-1}$) and Annual NCP (mol C m^{-2}·$year^{-1}$) in the mixed layer and whole water column

Category	R1	R2	R3W	R3E	Mainstem
Mixed layer NCP					
Autumn to winter	−0.21	0.06	0.03	−0.06	−0.04
Winter to spring	0.28	0.03	0.04	0	0.07
Spring to summer	−0.01	0.19	0.03	0.14	0.11
Annual	0.18	0.65	0.27	0.10	0.31
Whole water column NCP					
Autumn to winter	−0.22	−0.06	−0.01	−0.03	−0.07
Winter to spring	−0.11	−0.06	−0.04	−0.04	−0.06
Spring to summer	−0.20	−0.09	−0.02	0.05	−0.05
Annual	−1.4	−0.54	−0.19	−0.11	−0.48

Note. The uncertainty associated with NCP in the surface and subsurface waters are 0.08 mol C m^{-2}·$month^{-1}$ and 0.07 mol C m^{-2}·$month^{-1}$, respectively. Δt between autumn and winter and winter and spring was 3 months and Δt between spring and summer was 2 months.
Abbreviation: NCP = net community production.

estimate when it is scaled to a comparable surface area of Feng et al. (2015) that similarly includes both the tributaries and the mainstem (3.7×10^{10} g C $year^{-1}$). NCP was computed for a period of 5 years and varied by an order of magnitude in the Feng et al. (2015) study, indicating that interannual variability, and not only seasonality, plays a large role in dictating the trophic status of a system. A recent modeling analysis based on a 30-year time period also concluded that the CB main stem is net autotrophic (Shen, Testa, Ni, et al., 2019; Shen, Testa, Li, 2019). Finally, both Najjar et al. (2018) and Herrmann et al. (2015) classified the CB as net autotrophic, despite their conclusion that the majority of estuarine systems on the east coast of the United States are heterotrophic. The results of this study, however, indicate that the whole water column of the CB mainstem during the 2016/2017 study period is net heterotrophic, suggesting the region may behave more similarly to other east coast estuaries.

5. Summary and Conclusions

This study examined the variability of the CO_2 system throughout the CB mainstem over a complete seasonal cycle. Using 17 stations, subdivided into four geographic regions, the seasonality of DIC, pH, and pCO_2 were examined. Regardless of season, latitudinal gradients of both DIC and TA were observed in the surface mixed layer, with lowest concentrations observed in the northern CB near the mouth of the Susquehanna River and highest concentrations observed at the mouth of the CB where estuarine waters closely interact with Atlantic Ocean shelf waters. The accumulation of DIC-rich waters at depth, coincident with periods of seasonal stratification and temperature-dependent remineralization, are likely to exacerbate ocean acidification in this coastal system. In the seasonally stratified northern CB mainstem, surface waters are undersaturated with respect to atmospheric CO_2 year-round resulting from a dominance of the removal of CO_2 by photosynthesis over thermally driven changes in pCO_2. In contrast, surface waters in the lower CB experience seasonal CO_2 outgassing or neutral conditions as the thermally driven increase in pCO_2 outweighs the biologically driven removal of DIC as the productive season declines. The CB mainstem was a net sink for atmospheric CO_2 on the order of 0.38 mol C m^{-2}·$year^{-1}$. A mass balance of DIC indicates that when scaled to the surface area of the mainstem, the mixed layer was net autotrophic, with a net community production of 0.31 mol C m^{-2} $year^{-1}$, and that the whole water column was heterotrophic, with an NCP of −0.48 mol C m^{-2} $year^{-1}$. Because interannual variability in this dynamic nearshore system is likely to be large, continued monitoring of the CO_2 system should be prioritized. Since changes driven by the increase in anthropogenic CO_2 are small compared to natural variability, the work presented here represents a crucial step in understanding the evolution of the system in response to climate change.

Acknowledgments
Funding was provided by the National Science Foundation via grants OCE-1537013 and OCE-1536996. We are grateful to the NOAA Chesapeake Bay office for their assistance and collaboration, as well as John Donat and Mark Trice for their collaboration with the Chesapeake Bay Monitoring Program. This is VIMS manuscript 3866; data are available at William & Mary's ScholarWorks doi: https://doi.org/10.25773/rntn-ez18

References

Borges, A. V. (2005). Do we have enough pieces of the jigsaw to integrate CO_2 fluxes in the coastal ocean? *Estuaries*, *28*(1), 3–27. https://doi.org/10.1007/BF02732750

Brodeur, J. R., Chen, B., Su, J., Xu, Y.-Y., Husstain, N., Scaboo, K. M., et al. (2019). Chesapeake Bay inorganic carbon: spatial distribution and seasonal variability. *Frontiers in Marine Science*, *6*, 99. https://doi.org/10.3389/fmars.2019.00099

Cai, W., Dai, M., Wang, Y., Zhai, W., Huang, T., Chen, S., et al. (2004). The biogeochemistry of inorganic carbon and nutrients in the Pearl River estuary and the adjacent northern South China Sea. *Continental Shelf Research*, *24*(12), 1301–1319. https://doi.org/10.1016/j.csr.2004.04.005

Cai, W.-J., Hu, X., Huang, W.-J., Murrell, M. C., Lehrter, J. C., Lohrenz, S. E., et al. (2011). Acidification of subsurface coastal waters enhanced by eutrophication. *Nature Geoscience*, *4*(11), 766–770. https://doi.org/10.1038/ngeo1297

Cai, W.-J., Huang, W.-J., Luther, G. W., Pierrot, D., Li, M., Testa, J., et al. (2017). Redox reactions and weak buffering capacity lead to acidification in the Chesapeake Bay. *Nature Communications*, *8*(1), 369. https://doi.org/10.1038/s41467-017-00417-7

Chesapeake Bay Program. (2004). Chesapeake Bay Program Analytical Segmentation Scheme—Revision, decisions and rationals 1983-2003.

Chesapeake Bay Program. (2012). Guide to using Chesapeake Bay program water quality monitoring data.

Da, F., Friedrichs, M. A. M., & St-Laurent, P. (2018). Impacts of atmospheric nitrogen deposition and coastal nitrogen fluxes on oxygen concentrations in Chesapeake Bay. *Journal of Geophysical Research: Oceans*, *123*, 5004–5025. https://doi.org/10.1029/2018JC014009

Dickson, A. G. (1990). Standard potential of the reaction: $AgCl(s) + 12H_2(g) = Ag(s) + HCl(aq)$, and the standard acidity constant of the ion HSO_4^- in synthetic sea water from 273.15 to 318.15 K. *The Journal of Chemical Thermodynamics*, *22*(2), 113–127. https://doi.org/10.1016/0021-9614(90)90074-Z

Dickson, A. G., & Millero, F. J. (1987). A comparison of the equilibrium constants for the dissociation of carbonic acid in seawater media. *Deep Sea Research Part A, Oceanographic Research Papers*, *34*(10), 1733–1743. https://doi.org/10.1016/0198-0149(87)90021-5

Doney, S. C. (2010). The growing human footprint on coastal and open-ocean Bbogeochemistry. *Science*, *328*(5985), 1512–1516. https://doi.org/10.1126/science.1185198

Doney, S. C., Fabry, V. J., Feely, R. A., & Kleypas, J. A. (2009). Ocean acidification: The other CO_2 problem. *Annual Review of Marine Science*, *1*(1), 169–192. https://doi.org/10.1146/annurev.marine.010908.163834

Dore, J. E., Lukas, R., Sadler, D. W., Church, M. J., & Karl, D. M. (2009). Physical and biogeochemical modulation of ocean acidification in the central. *North Pacific*, *106*(30), 12,235–12,240. https://doi.org/10.1073/pnas.0906044106

Feng, Y., Friedrichs, M. A. M., Wilkin, J., Tian, H., Yang, Q., Hofmann, E. E., et al. (2015). Chesapeake Bay nitrogen fluxes derived from a land-estuarine ocean biogeochemical modeling system: Model description, evaluation, and nitrogen budgets. *Journal of Geophysical Research: Biogeosciences*, *120*, 1666–1695. https://doi.org/10.1002/2015JG002931.Received

Goodrich, D. M., & Blumberg, A. F. (1991). The fortnightly mean circulation of chesapeake bay. *Estuarine, Coastal and Shelf Science*, *32*(5), 451–462. https://doi.org/10.1016/0272-7714(91)90034-9

Hagy, J. D., Bonton, W. R., Keefe, C. W., & Wood, K. V. (2004). Hypoxia in Chesapeake Bay, 1950-2001: Long-term change in relation to nutrient loading and river flow. *Estuaries*, *27*(4), 634–658. https://doi.org/10.1007/BF02907650

Harding, L. W., Adolf, J. E., Mallonee, M. E., Miller, W. D., Gallegos, C. L., Perry, E. S., et al. (2014). Climate effects on phytoplankton floral composition in Chesapeake Bay. *Estuarine, Coastal and Shelf Science*, *162*, 53–68. https://doi.org/10.1016/j.ecss.2014.12.030

Harding, L. W., Gallegos, C. L., Perry, E. S., Miller, W. D., Adolf, J. E., Mallonee, M. E., & Paerl, H. W. (2016). Long-term trends of nutrients and phytoplankton in Chesapeake Bay. *Estuaries and Coasts*, *39*(3), 664–681. https://doi.org/10.1007/s12237-015-0023-7

Herrmann, M., Najjar, R. G., Kemp, W. M., Alexander, R. B., Boyer, E. W., Cai, W.-J., et al. (2015). Net ecosystem production and organic carbon balance of U.S. East Coast estuaries: A syntheiss approach. *Global Biogeochemical Cycles*, *29*, 96–111. https://doi.org/10.1002/2013GB004736

Hiscock, W. T., & Millero, F. J. (2006). Alkalinity of the anoxic waters in the Western Black Sea. *Deep Sea Research Part II: Topical Studies in Oceanography*, *53*(17-19), 1787–1801. https://doi.org/10.1016/j.dsr2.2006.05.020

Hu, X., Li, Q., Huang, W., Chen, B., Cai, W., Rabalais, N. N., & Turner, R. E. (2017). Effects of eutrophication and benthic respiration on water column carbonate chemistry in a traditional hypoxic zone in the Northern Gulf of Mexico. *Marine Chemistry*, (November 2016, *194*, 33–42. https://doi.org/10.1016/j.marchem.2017.04.004

Irby, I. D., Friedrichs, M. A. M., Friedrichs, C. T., Bever, A. J., Hood, R. R., Lanerolle, L. W. J., et al. (2016). Challenges associated with modeling low-oxygen waters in Chesapeake Bay: A multiple model comparison. *Biogeosciences*, *12*(24), 20,361–20,409. https://doi.org/10.5194/bgd-12-20361-2015

Joesoef, A., Huang, W. J., Gao, Y., & Cai, W. J. (2015). Air-water fluxes and sources of carbon dioxide in the Delaware Estuary: Spatial and seasonal variability. *Biogeosciences*, *12*(20), 6085–6101. https://doi.org/10.5194/bg-12-6085-2015

Joesoef, A., Kirchman, D. L., Sommerfield, C. K., & Cai, W. (2017). Seasonal variability of the inorganic carbon system in a large coastal plain estuary. *Biogeosciences*, *14*(21), 4949–4963. https://doi.org/https://doi.org/10.5194/bg-14-4949-2017

Kemp, W. M., Smith, E. M., Marvin-DiPasquale, M., & Boynton, W. R. (1997). Organic carbon balance and net ecosystem metabolism in Chesapeake Bay. *Marine Ecology Progress Series*, *150*(1–3), 229–248. https://doi.org/10.3354/meps150229

Laruelle, G. G., Lauerwald, R., Rotschi, J., Raymond, P. A., Hartmann, J., & Regnier, P. (2015). Seasonal response of air-water CO_2 exchange along the land-ocean aquatic continuum of the northeast North American coast. *Biogeosciences*, *12*(5), 1447–1458. https://doi.org/10.5194/bg-12-1447-2015

Laruelle, G. G., Dürr, H. H., Slomp, C. P., & Borges, A. V. (2010). Evaluation of sinks and sources of CO_2 in the global coastal ocean using a spatially-explicit typology of estuaries and continental shelves. *Geophysical Research Letters*, *37*, L15607. https://doi.org/10.1029/2010GL043691

Mehrbach, C., Culberson, C., Hawley, J., & Pytkowicz, R. (1973). Measurement of the apparent dissociation constants of carbonic-acid in seawater at atmospheric pressure. *Limnology and Oceanography: Methods*, *18*(November(6), 897–907. https://doi.org/10.4319/lo.1973.18.6.0897

Najjar, R. G., Herrmann, M., Alexander, R., Boyer, E. W., Burdige, D. J., Butman, D., et al. (2018). Carbon budget of tidal wetlands, estuaries, and shelf waters of eastern North America. *Global Biogeochemical Cycles*, *32*(3), 389–416. https://doi.org/10.1002/2017GB005790

Nightingale, P. D., Malin, G., Law, C. S., Watson, A. J., Liss, P. S., Liddicoat, M. I., et al. (2000). In situ evaluation of air-sea gas exchange parameterizations using novel conservative and volatile tracers. *Global Biogeochemical Cycles*, *14*(1), 373–387. https://doi.org/10.1029/1999GB900091

Orr, J. C., Fabry, V. J., Aumont, O., Bopp, L., Doney, S. C., Feely, R. A., et al. (2005). Anthropogenic ocean acidification over the twenty-first century and its impact on calcifying organisms. *Nature*, *437*(7059), 681–686. https://doi.org/10.1038/nature04095

Raymond, P. A., Bauer, J. E., & Cole, J. J. (2000). Atmospheric CO_2 evasion, dissolved inorganic carbon production, and net heterotrophy in the York River estuary. *Limnology and Oceanography*, *45*(8), 1707–1717. https://doi.org/10.4319/lo.2000.45.8.1707

Reay, W. G. (2009). Water quality within the York River Estuary. *Journal of Coastal Research*, *57*, 23–39. https://doi.org/10.2112/1551-5036-57.sp1.23

Schneider, B. (2011) The CO_2 System of the Baltic Sea: Biogeochemical Control and Impact of Anthropogenic CO_2. In G. Schernewski, J. Hofstede, & T. Neumann (Eds.). *Global Change and Baltic Coastal Zones. Coastal Research Library* (Vol 1). Springer, Dordrecht.

Schultz, G. E. (1999). Bacterial dynamics and community structure in the York River estuary. https://doi.org/10.25773/v5-e0ce-tt62

Shadwick, E. H., Friedrichs, M. A. M., Najjar, R. G., De Meo, O. A., Friedman, J. R., Da, F., & Reay, W. G. (2019). High frequency CO_2 system variability over the winter-to-spring transition in a coastal plain estuary. *Journal of Geophysical Research: Oceans*, *124*, 7626–7642. https://doi.org/10.1029/2019JC015246

Shadwick, E. A., De Meo, O. A., & Friedman, J. R. (2019). Discrete CO_2-System Measurements in the Chesapeake Bay Mainstem between 2016 and 2018.

Shadwick, E. H.,Thomas, H., Azetsu-Scott, K., Greenan, B. J. W., Head, E., & Horne, E. (2011). Seasonal variability of dissolved inorganiccarbon and surface water pCO_2 in the Scotian Shelf region of the Northwestern Atlantic. *Marine Chemistry*, *124*, 23–37. https://doi.org/10.1016/j.marchem.2010.11.004

Sharp, J. H., Culberson, C. H., & Church, T. M. (1982). The chemistry of the Delaware estuary, general considerations. *Limnology and Oceanography*, *27*(6), 1015–1028. https://doi.org/10.4319/lo.1982.27.6.1015

Shen, C., Testa, J. M., Ni, W., Cai, W.-J., Li, M., & Kemp, W. M. (2019). Ecosystem metabolism and carbon balance in Chesapeake Bay: A 30-year analysis using a coupled hydrodynamic-biogeochemical model. *Journal of Geophysical Research: Oceans*, *124*, 6141–6153. https://doi.org/10.1029/2019JC015296

Shen, C., Testa, J., Li, M., Cai, W.-J., Waldbusser, G. G., Ni, W., et al. (2019). Controls on carbonate system dynamics in a coastal plain estuary: A modeling study. *Journal of Geophysical Research: Biogeosciences*, *124*, 61–78. https://doi.org/10.1029/2018JG004802

Sin, Y., Wetzel, R. L., & Anderson, I. C. (1999). Spatial and temporal characteristics of nutrient and phytoplankton dynamics in the York River Estuary, Virginia: Analyses of long-term data. *Estuaries*, *22*(2), 260–275. https://doi.org/10.2307/1352982

Sunda, W. G., & Cai, W. J. (2012). Eutrophication induced CO_2-acidification of subsurface coastal waters: Interactive effects of temperature, salinity, and atmospheric pCO_2. *Environmental Science and Technology*, *46*(19), 10,651–10,659. https://doi.org/10.1021/es300626f

United States Geological Survey (2018). Freshwater Flow into the Chesapeake Ba. https://www.usgs.gov/centers/cba/science/freshwater-flow-chesapeake-bay?qt-science_center_objects=1#qt-science_center_objects

Vandemark, D., Salisbury, J. E., Hunt, C. W., Shellito, S., & Irish, J. (2011). Temporal and spatial dynamics of CO_2 air-sea flux in the Gulf of Maine. *Journal of Geophysical Research*, *116*, C01012. https://doi.org/10.1029/2010JC006408

van Heuven, S., Pierrot, D., Rae, J. W. B., Lewis, E., & Wallace, D. W., (2011). MATLAB Program Developed for CO_2 System Calculations, Tech. rep., ORNL/CDIAC.

Waldbusser, G. G., & Salisbury, J. E. (2014). Ocean acidification in the coastal zone from an organism's perspective: Multiple system parameters, frequency domains, and habitats. *Annual Review of Marine Science*, *6*(1), 221–247. https://doi.org/10.1146/annurev-marine-121211-172238

Wanninkhof, R. (2014). Relationship between wind speed and gas exchange over the ocean revisited. *Limnology and Oceanography: Methods*, *12*(6), 351–362. https://doi.org/10.4319/lom.2014.12.351

Wanninkhof, R., & McGillis, W. R. (1999). A cubic relationship between air-sea CO_2 exchange and wind speed. *Geophysical Research Letters*, *26*(13), 1889–1892. https://doi.org/10.1029/1999GL900363

Weiss, R. F. (1974). Carbon dioxide in water and seawater: The solubility of a non-ideal gas. *Marine Chemistry*, *44*(4), 1148–1154. https://doi.org/10.4319/lo.1999.44.4.1148

Zimmerman, A. R., & Canuel, E. A. (2000). A geochemical record of eutrophication and anoxia in Chesapeake Bay sediments: Anthropogenic influence on organic matter composition. *Marine Chemistry*, *69*(1–2), 117–137. https://doi.org/10.1016/S0304-4203(99)00100-0